




# Electrical performance and reliability assessment of silver inkjet printed circuits on flexible substrates

Mohd Afiq Mohd Asri<sup>1</sup> , Noor Amalina Ramli<sup>1</sup>, and Anis Nurashikin Nordin<sup>1,\*</sup> 

<sup>1</sup>Department of Electrical and Computer Engineering, International Islamic University Malaysia, Gombak, 53100 Kuala Lumpur, Malaysia

**Received:** 16 January 2021

**Accepted:** 6 May 2021

**Published online:**  
29 May 2021

© The Author(s), under exclusive licence to Springer Science+Business Media, LLC, part of Springer Nature 2021

## ABSTRACT

Inkjet printing has proven to be a promising alternative method in the fabrication of printed electronics, besides screen printing and photolithography etching. In this work, we characterize the electrical performance of inkjet printed circuits on flexible PET and glossy photo paper. The electrical circuits were printed using a commercial Epson L310 piezoelectric printer, and the NB series silver ink and chemical-sintering PET substrate from Mitsubishi Paper Mills. This method allows rapid prototyping of electronic circuits (~ 30 min design, ~ 5 s fabrication) and quick iteration of prototypes. The system has a resolution of 250  $\mu\text{m}$  electrodes and 300  $\mu\text{m}$  electrical gaps, and on average,  $1.5 \pm 0.2 \mu\text{m}$  in thickness. The effect of printing on different substrates, geometry and overprinting on sheet resistance was also studied. It was found that double printing produced better electrodes with lower resistances. A stable conducting circuit has a sheet resistivity of  $< 150 \text{ m}\Omega/\text{sq}$  for high aspect ratio features such as wires, and horizontal patterns have higher conductivities compared to vertical patterns. Optimum gap between conducting lines was found to be 300  $\mu\text{m}$  with smaller gaps creating stray ink blotches that cause short circuits. The printed lines are tolerant against common solvents and conduct reliably when operating under 100 °C. For bending tests, a serpentine flexion sensor was printed and bent at angles from  $-90^\circ$  to  $90^\circ$ . It was found that at reverse bending, the resistivity increases 0.9% for every  $1^\circ$  bent while for forward bending, the resistivity decreases by the sum of 0.4% for every  $1^\circ$  bent. The printed circuits are resistant to the Scotch tape test, immersion in deionized water, acetone and ethyl alcohol with line resistance still within less than 10  $\Omega/\text{cm}$  after treatment. This study shows that silver inkjet printed electrodes can be reliably printed using a commercial printer to produce low-cost flexible and wearable electronics.

Address correspondence to E-mail: anisnn@iiium.edu.my

## 1 Introduction

Recent advances in emerging electronic technologies such as biosensors, wearable electronics, flexible electronics, microelectromechanical systems (MEMS) and the Internet of Things (IoT) spurred the rapid improvements of new and existing on-demand fabrication techniques for electronic circuits. In addition to the traditional photolithographic printed circuit board (PCB) and thin-film microfabrication methods used in the production of circuit boards and integrated circuits, some novel techniques include computer numerical control (CNC) copper milling, aerosol deposition, selective laser sintering (SLS), contact printing (such as gravure and flexographic press printing), roll-to-roll printing, and noncontact printing (such as screen printing and inkjet printing) [1–3]. On-demand fabrication is of particular importance for electronics hardware developers within academia and industry, as well as public hobbyists. Among these techniques, screen printing and inkjet printing are increasingly popular for rapid prototyping of electronic circuits, due to its relatively low cost and ease of access to fabrication tools. These methods involve the patterning and deposition of conductive material—commonly metal or polymer in paste or colloidal solution—onto a substrate [1, 3].

Screen printing has several obvious advantages for circuit fabrication: it is a speedy process for mass production, has many types of printing materials available and allows multilayered device architectures of different materials. However, screen printing is not without disadvantages. These include low spatial resolution, relatively high material waste, requiring ad hoc masks for patterning, and operator-dependent reproducibility [4]. In the development of proofs-of-concept, these disadvantages increase turnaround time between iterations and likely involve more optimization work. Alternative approaches such as laser-induced graphitization (LIG) on polyimide enable a rapid and low-cost formation of electrical traces [5–7]; however, circuits made of carbon have high impedance, which contributes to poor performance when used in high-frequency applications such as antennas. LIG circuits often need to be supplemented with metal coating. Inkjet printing (IJP), at a glance, costs higher due to more expensive colloidal ink, is more restricted in its availability of functional materials and is a low-speed

process at mass production scale. However, IJP makes it up with better spatial resolution, higher repeatability, does not require masks, and consumes much less ink material per square unit of circuitry [4]. Further, IJP is also suitable for depositing both conductive materials and biological materials on substrates in a uniform manner [8]. These features merit the IJP method as the preferred choice for early-phase rapid prototyping, where short turnaround time between iteration is desirable, resources are limited, failure rates are often high, and the design evolves frequently.

Current works in our research group use screen printing for biosensors and flexible electronics fabrication. In addition, we also use Dimatix DMP-2800 research-grade inkjet printing system to experiment on silver-based inkjet-printed electrodes [9]. Similar system has been used in applications such as biosensors [10, 11], photovoltaic cells [12], soft matter electronics [13, 14], wearable electronics [15, 16], and thin-film transistors [17]. While research-grade IJP systems like Dimatix are widely utilized in printed electronics due to its high spatial resolution, reproducibility and versatility of ink and substrate materials [18–20], the start-up and maintenance cost is relatively expensive for a piece of commercial equipment. Furthermore, it requires specialized ink for each type of substrate, and the associated ink usually requires heat sintering at high temperatures [21]. This heat-sintering process adds additional fabrication time and may affect upstream treatments of any heat-sensitive surface chemistry.

Due to these shortcomings of research-use printers, alternative methods have been explored to exploit the advancements in drop-on-demand printhead technology of consumer printers. Office-use consumer printers are, on average, 1/250 of the cost of a research-grade multimaterial printer. While the variety of deposited materials and substrates is significantly reduced and the control over droplet size is compromised, office-use printers offer a viable option for metallic ink circuits. Both thermal and piezoelectric inkjet printers have been explored; however, piezoelectric printers are favored when used with colloidal conductive particles [22].

Kawahara and colleagues have developed a low-cost and reliable system for printing silver-based flexible circuits on piezoelectric consumer printers. The team utilized a chemical-sintered, water-based silver nanoparticle (AgNP) ink system and its

corresponding substrate developed by Mitsubishi Paper Mills that allows instant circuit patterning and AgNP sintering at room temperature [23]. They have demonstrated using the system to build liquid-level sensors, multi-touch sensors and wearable electronics within several hours of prototyping [24, 25]. More recently, they developed an origami soft robotics application through IJP [26]. Besides Mitsubishi Paper Mills, other major manufacturers of office printer-compatible silver inkjet printing systems include Novacentrix and AgIC. These inks typically work in tandem with specially developed flexible substrates, coated with resin that allows rapid sintering of the ink upon contact. The instant inkjet circuits have been used in applications spanning across point-of-care diagnostics [27, 28], chemical sensors [29], gas sensors [30], accelerometers [31] and antennas [32, 33]. The comparison of costs and iteration time between the methods is summarized in Table S1.

Several prior works have experimentally assessed the performance of instant inkjet printed circuits across various parameters. A common approach to studying sheet resistivity is through van der Pauw method [34, 35]. Joubert et al. studied effects of different printing substrates and sintering temperatures [36]. Albrecht and colleagues investigated the reduction of sheet resistivity during postprocessing by sintering using high-energy photon pulses [37]. Beisteiner and Zagar conducted a thorough characterization of printed sensors properties, covering thermoelectric effects, thermal-resistive effects, strain and pressure effects, surface passivation, and mechanical adhesion [38]. All these characterization works have featured either light microscopy- or scanning electron microscopy-based optical characterization, and many featured surface topology analyses. Based on these prior characterization strategies, we replicated the silver nanoparticle ink-based inkjet printing system for printed electronics as established by Kawahara and colleagues and experimentally assessed baseline performance for selected parameters of the system. These baselines include its fabrication limits, its resistivity, its physicochemical stability, and effects of bending. We then demonstrate the system's ability to rapidly prototype simple electrodes at short turnaround time and low cost.

## 2 Methods

### 2.1 Materials

Commercial Epson L310 inkjet printer (3 pL minimum drop volume, 5760 dpi × 1440 dpi resolution) and resin-coated high-quality glossy photo paper are purchased online from a local site (Lazada Malaysia). NBSIJ-MU01 silver nanoparticle ink and NB-TP-3GU100 polyethylene terephthalate substrate (PET) with microporous Al<sub>2</sub>O<sub>3</sub>-PVA single-sided coating is purchased from Mitsubishi Paper Mills Ltd (US letter-sized 8.5" × 11"; Tokyo, Japan). MG8331 silver epoxy is purchased through Digi-key Electronics (MN, USA). Deionized (DI) water had a resistivity of 18 MΩ at 25 °C.

### 2.2 Installation of low-cost silver nanoparticle ink-based electrode printing system

NBSIJ-001 silver nanoparticle ink is loaded into the CMYK ink-tank of an Epson L310 inkjet printer in equal parts (25 mL per tank) through a 500 μm filter. Ink is pumped from the auxiliary tank into the cartridge through Epson L310 driver's built-in charging function for 20 min.

Designs are created in AutoCAD 1.5 (Autodesk Inc., San Rafael, CA) or Inkscape 0.91 (open-source available on GitLab, GNU General Public License v2.0), converted into.svg files, and printed onto either photo paper or NB-TP-3GU100-coated PET substrate. For doubly printed devices, care is taken to align the substrate using the printer's paper size selector to minimize pattern misalignment. Devices printed are cut with scissors to separate from the batch.

### 2.3 Sheet resistance and resolution characterization

To find the initial minimum conducting print limit, 20 mm trace wires were doubly printed with widths of 100 to 500 μm, in 50 μm increments. End-to-end resistances were measured. Electrode details were examined using Zeiss Lab.A1 Axio optical microscope (Carl Zeiss Microscopy, Thornwood, NY) at 1000 × magnification.

Squares and rectangles (defined as low aspect ratio features henceforth) of dimensions of 1 cm × 1 cm, 2 cm × 1 cm (horizontally and vertically printed),

3 cm × 1 cm (horizontally and vertically printed), 2 cm × 2 cm, 4 cm × 2 cm (horizontal), and 6 cm × 2 cm (horizontal) were printed singly and doubly, in triplicates (each replicate is fabricated separately, i.e., in different print queues). Additionally, trace wires (defined as high aspect ratio features henceforth) of 250, 300, 350, 400, 450, 500, 600, 700, 800, 900, 1000, 1200, 1400, 1600, 1800 and 2000 μm in width and 22.5 mm in length were fabricated. Resistivity values were measured end to end using Pro'sKit MT-1710 precision multimeter. Sheet resistance values were calculated from Eq. 1:

$$R_s = R_{\text{measured}} \left( \frac{W}{L} \right) \quad (1)$$

where  $R_s$  is sheet resistance,  $R_{\text{measured}}$  is measured resistivity,  $W$  is the width of electrode (perpendicular to direction of measurement), and  $L$  is length of electrode (parallel to direction of measurement).

For gap study, 1 mm width wires were printed in parallel with gaps 100, 200, 300, 400, 500 and 600 μm in between them. Resistance was measured between adjacent wires and is concluded to be nonconducting if resistance exceeds 15 kΩ. Fabrication and measurements were performed in triplicates.

## 2.4 Surface topology characterization

Interdigitated transducer (IDT) devices of the length 1 mm and the following width-gap combination were doubly printed in single replicates: 100 μm width—100 μm gap, 300 μm width—300 μm gap, 500 μm width—500 μm gap, and 1 mm width—1 mm gap. Surface profilometry (performed at Nanofabrication Laboratory, Malaysia-Japan International Institute of Technology, Kuala Lumpur) was performed using a Dektak profilometer, with the stylus run through the mid-section of the IDT. Actual electrode width and gap size measurements were extracted from the surface profilometry curves and compared against the initial digital design. Electrode height measurements were normalized by linearization and convolution functions, and values are extracted using a custom Python script.

## 2.5 Flexible property characterization

40 mm × 25 mm resistive double-turn serpentine strain gauges (gauge tracks 25 mm × 1 mm) were doubly printed on PET substrate. Bond pads were

connected to wires using MG8331 silver epoxy. Resistance was measured across the bond pads while bending the sensor across its mid-section at angles  $-75^\circ$  to  $75^\circ$ , with  $15^\circ$  increments. Measurements were performed in triplicates. Resistivity change was calculated against resistivity at  $0^\circ$  bending as Eq. 2:

$$\Delta R = \frac{R_{\text{measured}} - R_0}{R_0} \quad (2)$$

## 2.6 Physical and chemical stability

Doubly printed IDT devices were photographed prior to stability tests. For physical stability tests, the devices were either scratched with a coin or subject to repeated Scotch tape adhesion and removal for ten times. For chemical stability tests, devices were immersed in 10 mL of either DI water, 70% ethanol, or 100% acetone for 21 h. Devices were rinsed in water afterward. Posttest photographs were acquired, and before- and afterimages were compared by visual inspection. End-to-end resistance measurements were performed post-immersion to inspect for device conductivity.

## 2.7 Temperature dependence study

Straight wires (20 mm × 500 μm) were doubly printed and placed in an oven at temperatures of 30, 45, 60, 75, 90, 105, 120, 135, and 150 °C, respectively, for 30 min each. Pre- and post-baked resistances were measured, and resistance change was calculated using Eq. 2 as previously.

# 3 Results and discussion

## 3.1 Installation of low-cost silver nanoparticle ink-based electrode printing system

A silver ink-based fabrication strategy for rapid prototyping of electronic circuits on an office piezoelectric inkjet printer is presented, based on the works by Kawahara et al. [24] with slight modifications. An Epson L310 inkjet printer is loaded with NBSIJ-MU01 silver nanoparticle ink and reliably prints electronic circuits onto its companion coated PET substrate (Fig. 1). The total cost of the system

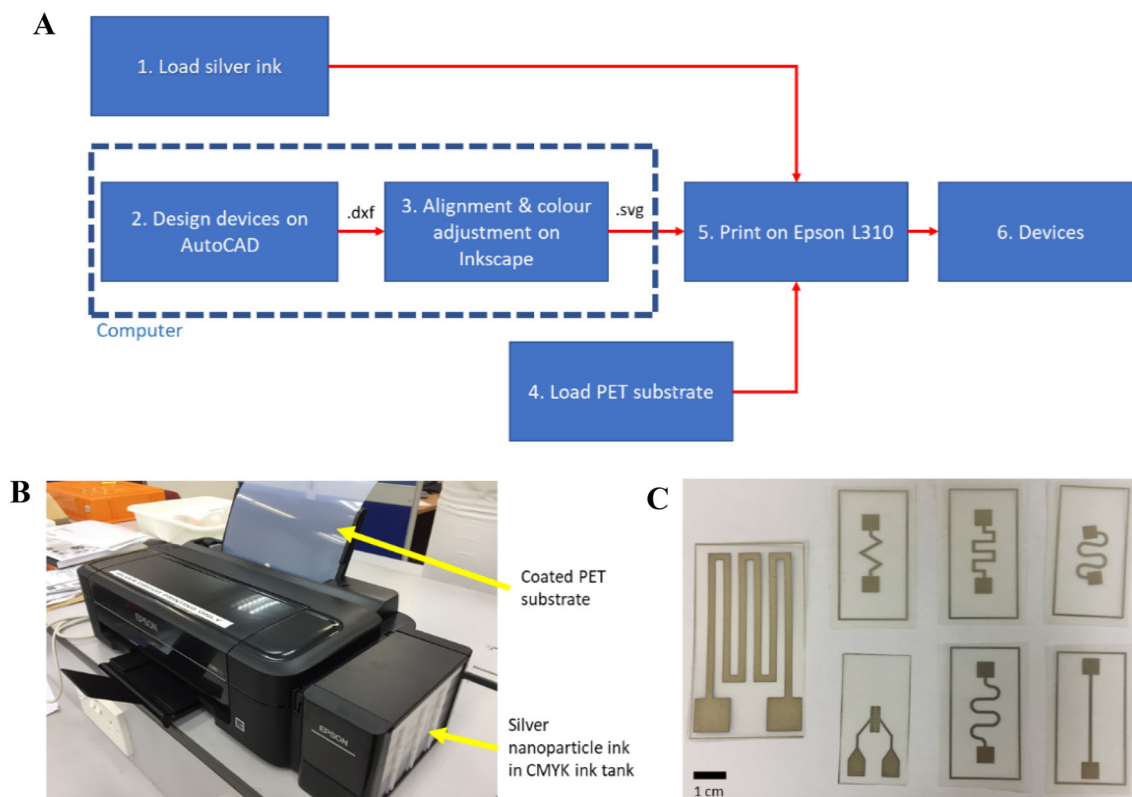


**Fig. 1** **a** Schematics of the silver inkjet printing process. **b** Silver circuit inkjet printing system. **c** Examples of printed devices

consisting of the printer, ink, and substrate, at the time of writing, is less than USD550 (MYR2250).

We discovered that Epson printers have a built-in function in its firmware that converts any color space format into RGB values, and then converting those values into CMYK color space [39]. Thus, we recommend that any designs are fed to the printer is set up in RGB colors that is converted into combinations of multiple CMYK colors (e.g. red (RGB 255, 0, 0); green (RGB 0, 255, 0); or blue (RGB 0, 0, 255)) to utilize combinations of multiple inkjet nozzles. For future works, it may be useful to attempt modification of the firmware to accept CYMK color space from the computer, to enable more control over silver ink consumption.

### 3.2 Effects of substrate, overprinting, and geometry on sheet resistance

Circuits that are printed over the coated PET substrate perform significantly better than the glossy photo paper substrate. Printing similar electrode designs over the substrate multiple times (*overprinting*) significantly improves its conductivity. To

conserve silver ink, it is discouraged to do this more than twice (*double-printed*). Furthermore, doubly printed devices are at risk of misalignment of the first printed pattern with the second printed pattern, where features smaller than 200  $\mu\text{m}$  can be lost if poorly aligned.

Sheet resistivity characteristics are measured and recorded (Table S2). Singly printed devices are found to potentially have major defects that could render it nonconducting, and its conductive devices perform 25 to 37 times worse than doubly printed devices. Observations under the microscope found that singly printed devices still have several holes in them, causing dielectric pockets within the device architecture (potentially air,  $\text{Al}_2\text{O}_3$ -PVA coating, PET, or combination of them). These pockets appear less in doubly printed devices, as shown in Figure S1. It is also found that the conductivity of the silver printed electrodes varies greatly when measured in parallel to the printing direction, versus measured perpendicular to the printing direction. Horizontal patterns conduct three times better than vertical patterns for singly printed features and 30% better for doubly printed features.

Interestingly, the geometry of electrodes also plays a significant role in the sheet resistance values. Low aspect ratio features such as squares and rectangles have average sheet resistances around 38 Ω/sq (relative standard deviation, RSD = 95.5%) for singly printed and 880 mΩ/sq (RSD = 44.0%) for doubly printed patterns (Table S2). A large RSD for singly printed patterns is expected, as poorly printed devices will have poor conductivity; however, occasionally singly printed devices will have print qualities as well as doubly printed counterparts. High aspect ratio features such as doubly printed 250 μm × 22.5 mm wire traces exhibit  $R_s$  values lower than 300 mΩ/sq (RSD = 18.3%). Reasons for this are not obvious, but likely due to a more defined electron trajectory in a high aspect ratio feature that would cause a shorter path of least resistance, compared to larger features. Measured line and sheet resistances for wire traces under 500 μm are listed in Table 1. An initial conductivity study finds that the reliable wire trace size that could reliably conduct electricity is between 250 and 300 μm, as shown in Table 1. An extended study for wire traces of sizes between 250 and 2000 μm reveals a steadily decreasing trend in resistivity across a 10 mm length wire as its line width decreases (Fig. 2).

### 3.3 Trace and gap resolution

An initial conductivity study across wire traces demonstrates that the minimal width for wires and interdigitated electrode finger that would reliably conduct electricity is 250 μm. End-to-end resistivity measurements for wires of width < 250 μm ranged in 90 kΩ cm<sup>-1</sup> and above, corresponding to sheet

resistances of > 10kΩ/sq (Table 1). Line resistance at 250 μm is measured at 12.24 Ω cm<sup>-1</sup> and decreases as the width increases. An extended replicate study to the one in Table 1 as shown in Fig. 2 shows that careful fabrication process can significantly reduce this value down to 7 Ω cm<sup>-1</sup>, and the earlier higher line resistance likely was due to it being printed without a nozzle cleaning print performed beforehand. Microscope observation shows that for wires thinner than 250 μm, there can exist several discontinuities on the silver trace (as shown in Fig. 3), which causes the traces to be nonconductive. Line resistance for wire traces > 400 μm appears to be decreasing linearly, suggesting 400 μm to be a practical minimum for wire trace sizes when applying to circuits that can be replicated reliably, although trace widths of 250 to 400 μm are possible to fabricate.

For electrical gap study, two adjacent wires are considered distinct if there is sufficiently high resistance between them to determine they are nonconducting. In this study, 15kΩ was arbitrarily chosen as a cutoff. For gap study, 300 μm gaps are the minimum gap size that reliably ensures electrical separation ( $n = 3$ ). Microscope observation shows that at the microscale, there might be stray ink blotches seeping from the wires into the gaps (as shown in Fig. 4 for 200 μm gaps) that connect adjacent wires electrically. We also noticed that while stray ink blotches may occur at any gap sizes by accident, the stray inks do not interfere with electrical isolation when gaps are > 300 μm. For future works, it might be useful to measure capacitance values across gaps, which we suspect is within the pF range and not measurable with our current instrumentation.

**Table 1** Line resistance and sheet resistivity for printed wire traces between 100 μm to 500 μm in the initial resolution screening

Wire trace width (μm)	Line resistance (Ω/cm)	Sheet resistivity (Ω/sq)
100	<b>3.310 M ± 1.432 M</b>	<b>33.1 k ± 14.3 k</b>
150	<b>750.4 k ± 168.1 k</b>	<b>11.3 k ± 2.52 k</b>
200	<b>94.9 k ± 189.2 k</b>	<b>19.0 k ± 37.8 k</b>
250	12.24 ± 2.25	0.306 ± 0.056
300	9.64 ± 3.14	0.289 ± 0.094
350	7.27 ± 1.10	0.291 ± 0.044
400	6.19 ± 0.60	0.279 ± 0.027
450	5.19 ± 1.25	0.259 ± 0.062
500	2.71 ± 0.11	0.136 ± 0.005
Average $R_{sheet}$ (widths > 250 μm)		0.263 ± 0.104

All wires are 22.5 mm in length, doubly printed, and fabricated and measured in triplicates. Bold highlighted cells show line resistances exceeding 10 kΩ, suggesting the wire is nonconductive

**Fig. 2** Line (a) and sheet (b) resistance curve for wires of lengths 250  $\mu\text{m}$  to 2000  $\mu\text{m}$  in the extended resolution study. Sheet resistivity is consistently under 200  $\text{m}\Omega/\text{sq}$  for all wires > 250  $\mu\text{m}$ . A transitional region between 400  $\mu\text{m}$  to 1200  $\mu\text{m}$  occurs where the sheet resistance shows decreasing trend from 150  $\text{m}\Omega/\text{sq}$  and levels off around 100  $\text{m}\Omega/\text{sq}$  for trace widths > 1200  $\mu\text{m}$ . Experiments are performed in triplicates, error bars indicate 1 standard deviation

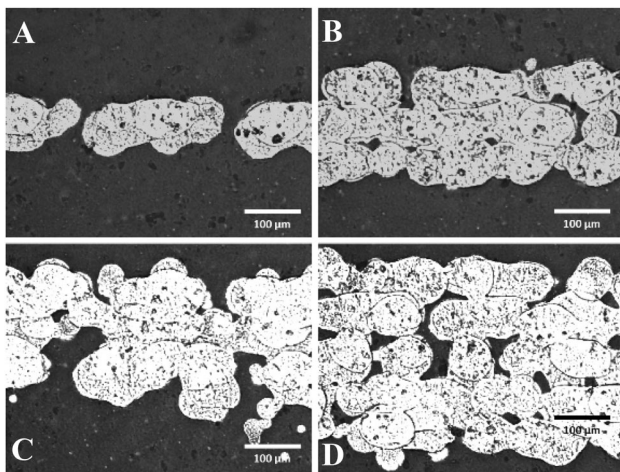
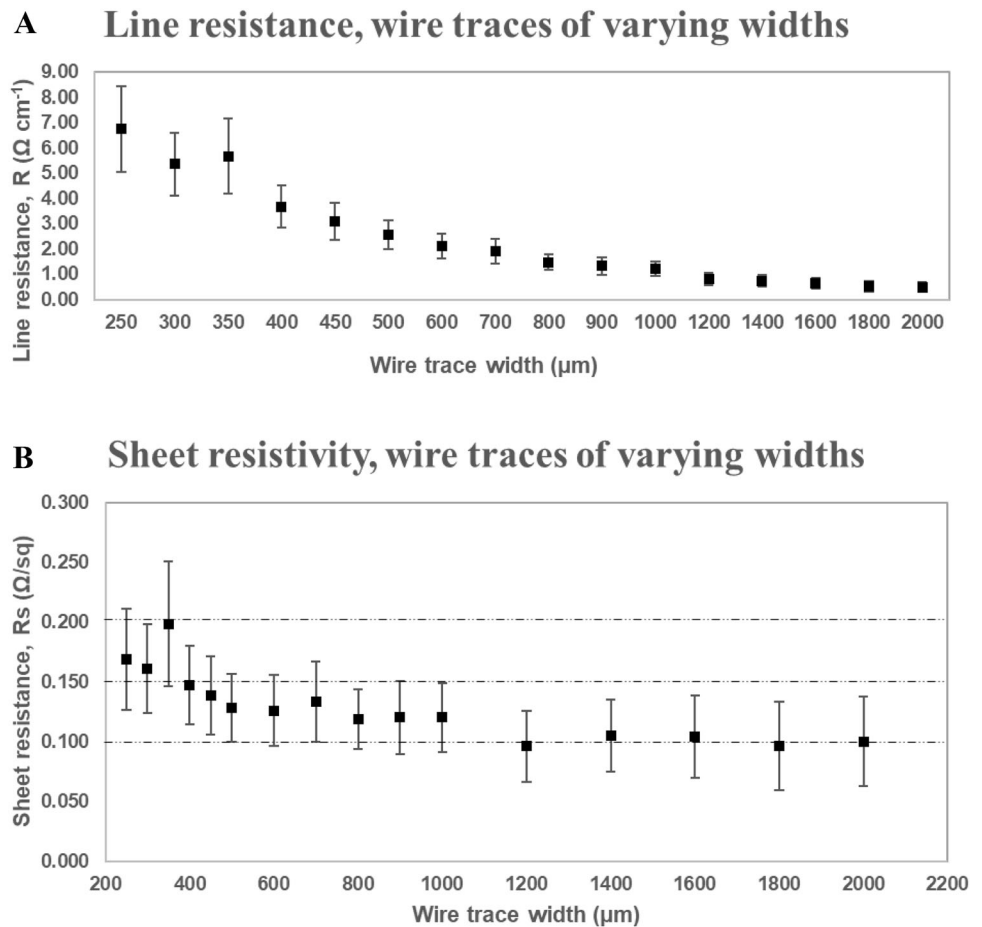


**Fig. 3** Representative light microscope images of wire traces under 1000  $\times$  magnification. **a** 100  $\mu\text{m}$  wires, **b** 200  $\mu\text{m}$  wires, **c** 300  $\mu\text{m}$  wires, **d**  $\mu\text{m}$  wires. Note that for 100  $\mu\text{m}$  wires, there exist very noticeable discontinuities within the wire architecture itself

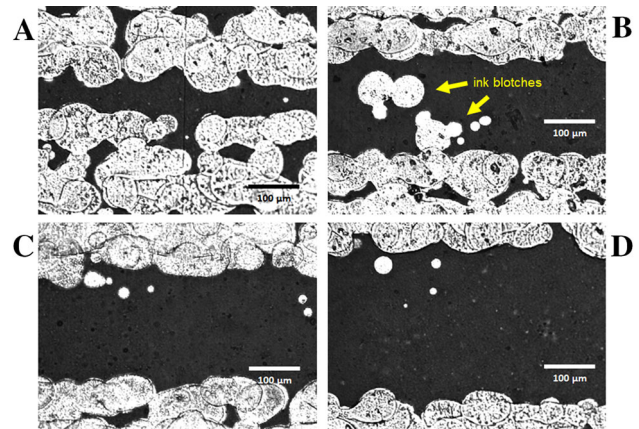


**Fig. 4** Representative light microscope images of wire gaps under 1000  $\times$  magnification. **a** 100  $\mu\text{m}$  gap, **b** 200  $\mu\text{m}$  gap, **c** 300  $\mu\text{m}$  gap, **d** 400  $\mu\text{m}$  gap. In 100  $\mu\text{m}$  gaps, the silver ink architecture is very close to each other and could potentially cause electrical coupling between the two adjacent wires. For 200, 300 and 400  $\mu\text{m}$  gaps, there are stray ink blotches inside the gaps (indicated by yellow arrows), in which for 200  $\mu\text{m}$  gaps, could potentially cause electrical connection between two adjacent wires

### 3.4 Circuit topology

Surface profilometry is performed on four sets of doubly printed IDT electrodes, with fingers and gaps of equal widths of 100 μm, 300 μm, 500 μm, and 1000 μm. The probe is run across the mid-section of the IDT, across two fingers and one gap. A custom Python script is used to find and estimate the points of transition between finger and gap, and to measure the widths of each finger and gap, and the mean and max Z-height of the fingers. The mean and max Z-height are used to estimate the overall thickness of a doubly printed device.

Figure 5 and Table 2 summarize the findings of the topological study. The max thickness of a doubly printed circuit is measured to be 1.5 μm (RSD = 19.77%), with an average of 870 nm (RSD = 11.04%). The widths of the fingers shrink by 7.8% compared to the original CAD design for 100 μm and expand by 3.6%, 1.5% and 8.1%, respectively, for 300 μm, 500 μm, and 1000 μm designs. Inversely, the widths of the gaps widen by 21.2% compared to the original CAD design for 100 μm and shrink 11.5%, 3.5%, and 3.9%, respectively, for 300 μm, 500 μm, and 1000 μm designs.

These findings show that inkjet printed circuit systems can reach even lower thicknesses of circuits compared to other systems, such as Dimatix-2800 inkjet printing system (~ 2 μm) and screen-printing techniques (~ 6 μm) [9]. The change in widths of the fingers and gaps can be attributed to the particle size of the silver ink, as well as ink distribution of the drop-on-demand printhead system based on given resolution, in which within the < 250 μm region the printer tends to underprint as compared to the CAD design, as we have seen from the resolution study. The increase in width of the fingers for designs > 300 μm can be attributed to at least two factors: overdeposition of ink by the printer, and microlevel misalignments during the doubly printing process.

### 3.5 Recommended print settings

For the purposes of fabrication of devices using the silver inkjet printer, the print settings in Table 3 are recommended.

### 3.6 Effects of bending on conductivity

As a quick demonstration of the instant inkjet circuits in practical applications, we fabricate simple

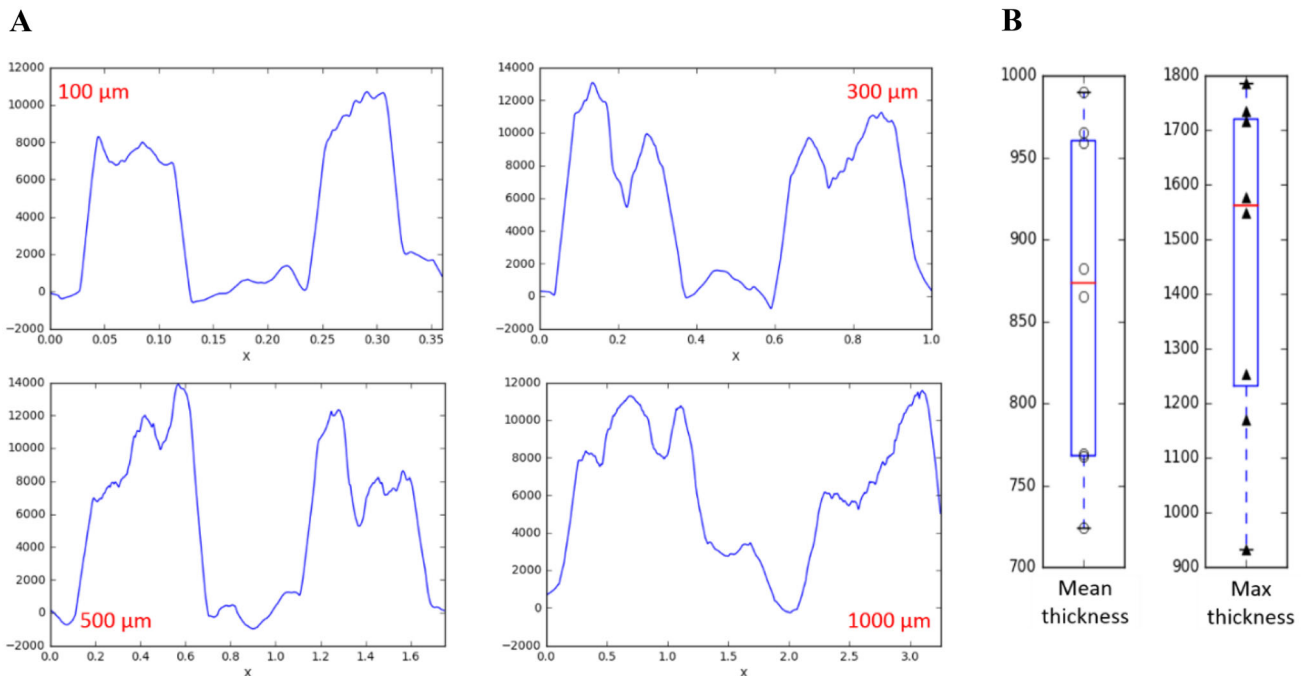


**Fig. 5 a** Topological profile of IDT fingers and gaps probed via surface profilometry. Representative region includes two adjacent fingers and one gap. Probe travel distance units are in millimeters,

Z-height units are in Angstroms. **b** Mean and max thickness of a doubly printed device, units in nanometers. Values are measured from the height of the IDT fingers



**Table 2** Change in finger and gap sizes between actual printed IDT devices versus digitally designed devices

CAD designed finger/gap size ( $\mu\text{m}$ )	$\Delta x/x$ (fingers)	$\Delta x/x$ (gaps)
100	− 0.078	+ 0.212
300	+ 0.036	− 0.115
500	+ 0.015	− 0.035
1000	+ 0.081	− 0.039
Mean finger height (nm), 8 samples		$865.25 \pm 95.52$
Max finger height (nm), 8 samples		$1464.90 \pm 289.54$

For 100  $\mu\text{m}$  fingers and gaps, the IDT fingers shrink in comparison with original CAD design, while the gaps expand in size. For 300  $\mu\text{m}$  onward, the IDT fingers widens while the gaps shrink. Mean and max finger height are based on eight measured fingers

**Table 3** Recommended print settings

Property	Values
Color	RGB red/green/blue (255, 0, 0), (0, 255, 0) or (0, 0, 255)
Substrate	Mitsubishi Paper Mills specially coated PET substrate
File format	Vector image -.svg,.pdf,.ai,.ppt
Overprinting	doubly-printed
Minimum wire size	250 $\mu\text{m}$
Minimum gap size	300 $\mu\text{m}$

serpentine resistive sensors that can quantify bend angles, which in theory can be incorporated into wearable sensor systems. While this application is simple, more complex applications such as complete printed circuit boards and RFID antenna have been demonstrated using the same system in precedent works [25].

A doubly printed resistive serpentine flexion sensor is bent in the forward direction (upward in the face direction of the circuit) at  $15^\circ$  angle increment, then returned to  $0^\circ$ . The sensor is then bent in the reverse direction (downward in the face direction of the circuit), then returned to  $0^\circ$ . The device and bending directions are portrayed in Fig. 6a and b. It is found that the forward bending best fits a profile of second-degree polynomial, while reverse bending fits a linear curve (Fig. 6c). At reverse bending, the resistivity increases 0.9% for every  $1^\circ$  bent ( $r^2 = 0.9906$ ). For forward bending, the resistivity decreases by the sum of 0.4% of  $\theta$  and 0.05% of  $\theta^2$  for every  $1^\circ$  bent ( $r^2 = 0.9969$ ).

After bending in both directions, the resistivity measurement at  $0^\circ$  shows that there is an upward trend in the baseline resistivity, suggesting that there may have been some irreversible damages to the silver particles' microstructure that causes an increase in resistance. This effect is small enough ( $< 6\%$  at the end of experiment) to warrant the use of

the silver printing as a printed circuit board, but the loss in precision over wear makes it less useful as mechanical sensors. A further study is required to explore bend angle boundaries such that the baseline resistivity change is negligible.

### 3.7 Physicochemical stability

Physicochemical stability of printed circuits against common physical conditions and solvents is explored. Sample devices were immersed in either DI water, 100% acetone, or 70% ethanol; or subjected to a Scotch tape test and a scratch test. Note that experiments were performed in a single replicate, and these results are preliminary. Table S3 shows the resultant pre- and posttreatment images of the devices. It is found that the devices are chemically stable in open immersion, able to withstand overnight immersion of water and common laboratory chemicals without degradation. It is also stable against adhesion-based removals, such as Scotch tapes. The circuits remain conductive after the treatment, with resistance values still within tolerable means. The silver ink, however, is not scratch tolerant. Against friction-based removal methods, the ink is easily removed.

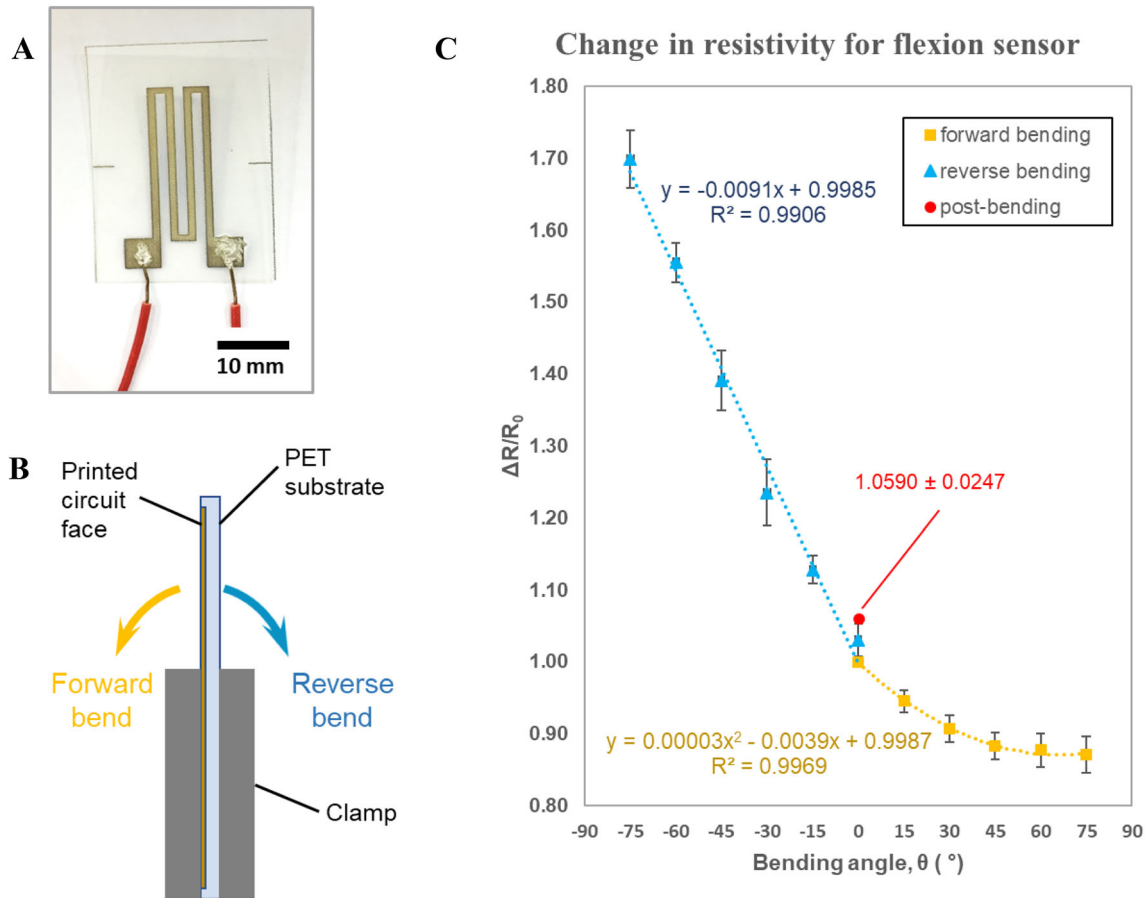


**Fig. 6** **a** Double-turn resistive serpentine flexion sensor. Bending angle is determined based on bending across the mid-section line. **b** Direction of bending for flexion sensor experiment. **c** Change in resistivity of at midpoint bending of double-turn serpentine resistive flexion sensors. Measurements are performed starting with forward bends (upward from the circuit face, square markers),

and then reverse bends (downward from the circuit face, triangular markers). An upward shift of  $\Delta R/R_0$  after bending in each direction (circular markers) suggests microscale damaging of the silver ink continuities beyond certain bending angles. Measurements are performed in triplicates, and error bars indicate 1 standard deviation

### 3.8 Effects of heat treatment on conductivity

Preliminary studies of circuit stability at varying temperatures were performed. Strips of PET containing  $500 \mu\text{m} \times 20 \text{mm}$  doubly printed straight wires were baked in oven at temperature ranges between 30 and 150 °C with 15 °C increments for 30 min each. The change of resistivity between pre- and post-baking is as shown in Figure S2. It was observed that at 90 °C, a mild warping of the PET substrate occurred. At 105 °C onward, permanent curling of PET was observed. The change in resistivity after heating is insignificant within temperature ranges of < 105 °C, which is well within the ranges of sensor electronics that do not involve high-heat environments. For actuator electronics that involve

resistive heating, further studies at higher temperature ranges are required. An interesting finding from this experiment is that somewhere between the 105 to 120 °C temperatures, the resistivity drops by 30% post-baking. Statistical analysis by Welch’s two-tailed t test yields a *p* value of 0.000116, which suggests that this difference is highly significant. This effect is possibly caused by temperature-dependent sintering of the silver nanoparticles as previously observed in a separate work [36]. The heat sintering improves conductivity and, however, adds processing lags to the otherwise instant fabrication time.

### 3.9 Comparison to other related studies

There have been various other studies characterizing aspects of inkjet printed silver circuits for both types

**Table 4** Summary of characterization studies involving electrical resistivity and geometry using commercial office printer-based instant inkjet circuit systems

References	Inkjet printing system	Sheet resistance (m $\Omega$ /sq)	Minimum trace width ( $\mu$ m)	Thickness ( $\mu$ m)
Kawahara et al. [24, 25]	Mitsubishi ink, Brother DCP-J140W printer	190–210	$\sim$ 200	n/a
Gieva et al. [34]	Novacentrix ink, Epson Stylus C88 + printer	4.08 (cross) 30.82 (square) 6.8 (disc)	n/a	n/a
Dixon et al. [27]	Novacentrix ink, Epson Stylus C88 + printer	n/a	150	1–1.25
Paracha et al. [33]	AgIC ink, Brother MFC-J430W printer	300	n/a	0.3
Albrecht et al. [37]	ANP ink, Epson Workforce 2010 W	385 90 (photon-sintered)	$\sim$ 150	$\sim$ 0.7
This work	Mitsubishi ink, Epson L310 printer	100–200	250	1.5

Values prefixed with a tilde (  $\sim$  ) indicate that the original study estimated the value through correlation with other known parameters in the study

of fabrication instruments (research-grade printers and commercial-grade printers). Here, we compare our work to several of commercial-grade printer-based systems. All the inks discussed in this section are compatible with commercial-grade printers, and the substrates are specially coated for chemical sintering with their corresponding silver ink.

Primarily, the benchmark work that we are comparing this project to is the original instant inkjet printed circuits study by Kawahara and colleagues [24, 25]. In that study, they found sheet resistance of the ink to be 210 m $\Omega$ /sq on average immediately after printing and improves to 190 m $\Omega$ /sq after 10 h. This is consistent with our findings where the sheet resistance is consistently under 200 m $\Omega$ /sq. It is also noted that Kawahara et al. used the same approach for calculating sheet resistance as our work. Gieva et al. [34] used the van der Pauw method to measure sheet resistances of instant inkjet circuits made using the Novacentrix commercial inkjet printing system (Metalon® JS-B25P ink, Novele™ substrate and Epson Stylus C88 + printer). The evaluated sheet resistances differ based on the geometry of the van der Pauw structure, which are 4.08 m $\Omega$ /sq for cross geometry, 30.82 m $\Omega$ /sq for square and 6.8 m $\Omega$ /sq for disc, respectively. While these values are significantly lower than the measured values from Kawahara and ours, it is important to note that the more expensive Novacentrix system advertised a lower resistivity (60–70 m $\Omega$ /sq) in their datasheet [40] as compared to

Mitsubishi's system (200 m $\Omega$ /sq); thus, these results are warranted. A separate work using AgIC silver inkjet printing system reports sheet resistance of 300 m $\Omega$ /sq [33]. Albrecht et al. used ANP's silver inkjet printing system and achieved sheet resistances of 385 m $\Omega$ /sq, but demonstrated that through photonic sintering at 734 kW for 750  $\mu$ s improves the sheet resistance to 90 m $\Omega$ /sq without damaging the circuits [37].

The thickness of the silver traces measured using profilometry yields similar results as a previous studies which also measured instant inkjet silver traces to be within the range of 1.0 to 1.3  $\mu$ m [27, 33]. The Dixon et al. study, however, demonstrated 150  $\mu$ m traces (designed at 100  $\mu$ m, with 50% expansion) using the Novacentrix system. This minimal trace width is smaller than our work, which may be attributed to the printer system. A separate study using SEM-based measurement reports 300 nm thickness for a AgIC ink-based printed circuit [33]. Table 4 summarizes these comparisons for geometries and electrical resistivity across the various works.

Two studies that performed extensive exploration for applications of instant inkjet circuits were Kawahara et al. and Beisteiner et al. [25, 38]. Kawahara and colleagues explored rapid PCB prototypes, flexible sensors, capacitive sensors, haptic interfaces and RFID tags. Beisteiner and Zagar explored thermocouples, temperature sensing, strain gauges and

pressure sensing. A common theme between these works with our work is through flexible/strain sensing, although it is difficult to compare side to side as the methods used are different (our work used angled bending method, Kawahara et al. used radius of curvature, Beisteiner et al. used lateral tensile stress); however, it can be observed that  $\Delta R/R_0$  consistently displays linear slope across all three types of measurement when stretched against the face of the silver patterns ('reverse bend' as defined in this paper). All three studies used silver ink from Mitsubishi Paper Mills.

## 4 Conclusion

We have successfully established and characterized a low-cost, functional and reproducible method to print electrical circuits onto pretreated flexible substrates using commercially available piezoelectric inkjet printer and silver nanoparticle ink. This work also includes early baseline characteristics to inform best practices when using the system. Using this method, it is possible to rapidly prototype circuits and printed electrodes at very low turnaround time (designing 10–30 min, fabrication  $\sim$  3 s). For circuit traces with widths  $>$  250  $\mu\text{m}$ , the sheet resistances are consistently under 200  $\text{m}\Omega/\text{sq}$ . This measurement is consistent with various independent studies in the literature. Preliminary investigations show that the circuits are chemically stable to common solvents, but are not scratch resistant. Circuits also operate stably at temperatures under 100  $^\circ\text{C}$ . Printability on flexible substrates, as well as predictable electrical variability displayed when bent, provides opportunities for in-house rapid fabrication of flexible electronics at a low cost.

## Acknowledgements

This project is financially supported by the Asian Office of Aerospace Research and Development. Additionally, N.A.R is supported by IIUM Research Initiative Grant for Post-Doctoral Fellows (IIUM, RPDF19-004-0014). The authors thank Ahmad Fairuzabadi Mohd Mansor for useful discussions. We thank Nabila Syafiq Abdul Rani for technical assistance with surface profilometry.

## Funding

This project is financially supported by the Asian Office of Aerospace Research and Development. Additionally, N.A.R is supported by IIUM Research Initiative Grant for Post-Doctoral Fellows (IIUM, RPDF19-004-0014).

## Declarations

**Conflict of interest** All the authors declared that they have no conflict of interest.

**Supplementary Information:** The online version contains supplementary material available at <http://doi.org/10.1007/s10854-021-06152-6>.

## References

1. S. Khan, L. Lorenzelli, R.S. Dahiya, Technologies for printing sensors and electronics over large flexible substrates: a review. *IEEE Sens. J.* **15**(6), 3164–3185 (2015). <https://doi.org/10.1109/JSEN.2014.2375203>
2. Q. Li et al., Review of printed electrodes for flexible devices. *Front. Mater.* **5**, 77 (2019). <https://doi.org/10.3389/fmats.2018.00077>
3. W. Wu, Inorganic nanomaterials for printed electronics: a review. *Nanoscale* **9**(22), 7342–7372 (2017). <https://doi.org/10.1039/C7NR01604B>
4. B. Andò, S. Baglio, A.R. Bulsara, T. Emery, V. Marletta, A. Pistorio, Low-cost inkjet printing technology for the rapid prototyping of transducers. *Sensors (Basel, Switzerland)* (2017). <https://doi.org/10.3390/s17040748>
5. J. Lin et al., Laser-induced porous graphene films from commercial polymers. *Nat. Commun.* **5**(1), 5714 (2014). <https://doi.org/10.1038/ncomms6714>
6. X. Tian et al., Dual-mode sensor and actuator to learn human-hand tracking and grasping. *IEEE Trans. Electron Devices* **66**(12), 5407–5410 (2019). <https://doi.org/10.1109/TED.2019.2949583>
7. J. Edberg, R. Brooke, O. Hosseinaei, A. Fall, K. Wijeratne, M. Sandberg, Laser-induced graphitization of a forest-based ink for use in flexible and printed electronics. *npj Flex Electron.* **4**(1), 17 (2020). <https://doi.org/10.1038/s41528-020-0080-2>
8. J. Li, F. Rossignol, J. Macdonald, Inkjet printing for biosensor fabrication: combining chemistry and technology for advanced manufacturing. *Lab. Chip* **15**(12), 2538–2558 (2015). <https://doi.org/10.1039/C5LC00235D>

9. A.A. Zainuddin, A.F.M. Mansor, R.A. Rahim, A.N. Nordin, Optimization of printing techniques for electrochemical biosensors. *AIP Conf. Proc.* **1808**, 020066 (2017). <https://doi.org/10.1063/1.4975299>
10. S. Carvajal et al., Disposable inkjet-printed electrochemical platform for detection of clinically relevant HER-2 breast cancer biomarker. *Biosens. Bioelectron.* **104**, 158–162 (2018). <https://doi.org/10.1016/j.bios.2018.01.003>
11. M. Trotter et al., Inkjet-printing of nanoparticle gold and silver ink on cyclic olefin copolymer for DNA-sensing applications. *Sensors* **20**(5), 1333 (2020). <https://doi.org/10.3390/s20051333>
12. K.Y. Mitra, A. Alalawe, S. Voigt, C. Boeffel, R.R. Baumann, Manufacturing of all inkjet-printed organic photovoltaic cell arrays and evaluating their suitability for flexible electronics. *Micromachines* **9**(12), 642 (2018). <https://doi.org/10.3390/mi9120642>
13. N. Adly et al., Printed microelectrode arrays on soft materials: from PDMS to hydrogels. *npj Flex Electron.* **2**(1), 15 (2018). <https://doi.org/10.1038/s41528-018-0027-z>
14. J. Byun et al., Fully printable, strain-engineered electronic wrap for customizable soft electronics. *Sci. Rep.* **7**(1), 45328 (2017). <https://doi.org/10.1038/srep45328>
15. S. Ali, S. Khan, A. Bermak, Inkjet-printed human body temperature sensor for wearable electronics. *IEEE Access* **7**, 163981–163987 (2019). <https://doi.org/10.1109/ACCESS.2019.2949335>
16. M. Gao, L. Li, Y. Song, Inkjet printing wearable electronic devices. *J. Mater. Chem. C* **5**(12), 2971–2993 (2017). <https://doi.org/10.1039/C7TC00038C>
17. K.Y. Mitra, M. Polomoshnov, C. Martínez-Domingo, D. Mitra, E. Ramon, R.R. Baumann, Fully inkjet-printed thin-film transistor array manufactured on paper substrate for cheap electronic applications. *Adv. Electron. Mater.* **3**(12), 1700275 (2017). <https://doi.org/10.1002/aelm.201700275>
18. D.D. Le, T.N.N. Nguyen, D.C.T. Doan, T.M.D. Dang, M.C. Dang, Fabrication of interdigitated electrodes by inkjet printing technology for application in ammonia sensing. *Adv. Nat. Sci.* **7**(2), 025002 (2016). <https://doi.org/10.1088/2043-6262/7/2/025002>
19. P.M. Grubb, H. Subbaraman, S. Park, D. Akinwande, R.T. Chen, Inkjet printing of high performance transistors with micron order chemically set gaps. *Sci. Rep.* **7**(1), 1202 (2017). <https://doi.org/10.1038/s41598-017-01391-2>
20. P.H. Bezuidenhout, K.J. Land, T.-H. Joubert, Integrating integrated circuit chips on paper substrates using inkjet printed electronics (2016). 17th Annual Conference of the Rapid Product Development Association of South Africa (RAPDASA), 2–4 November 2016, Vaal University of Technology
21. Silver Jet Ink | Nano-Silver Ink for Inkjet Printing | ANP Co., Ltd. [http://anapro.com/eng/product/silver\\_inkjet\\_ink.html](http://anapro.com/eng/product/silver_inkjet_ink.html). Accessed 19 Sept 2017
22. L. Gonzalez-Macia, A. Morrin, M.R. Smyth, A.J. Killard, Advanced printing and deposition methodologies for the fabrication of biosensors and biodevices. *Analyst* **135**(5), 845–867 (2010). <https://doi.org/10.1039/b916888e>
23. Silver Nano | Mitsubishi Paper Mills. <https://www.mpm.jp/electronic/eng/silver-nano/index.html>. Accessed 19 Sept 2017
24. Y. Kawahara, S. Hodges, N.-W. Gong, S. Olberding, J. Steimle, Building functional prototypes using conductive inkjet printing. *IEEE Pervasive Comput.* **13**(3), 30–38 (2014). <https://doi.org/10.1109/MPRV.2014.41>
25. Y. Kawahara, S. Hodges, B.S. Cook, C. Zhang, G.D. Abowd, Instant inkjet circuits: lab-based inkjet printing to support rapid prototyping of UbiComp devices. *Proceedings of the 2013 ACM international joint conference on Pervasive and ubiquitous computing - UbiComp '13*, (Zurich, Switzerland, 2013), p. 363. <https://doi.org/10.1145/2493432.2493486>
26. K. Nakahara, K. Narumi, R. Niiyama, Y. Kawahara, Electric phase-change actuator with inkjet printed flexible circuit for printable and integrated robot prototyping. (2017). <https://doi.org/10.1109/ICRA.2017.7989217>
27. C. Dixon, A.H.C. Ng, R. Fobel, M.B. Miltenburg, A.R. Wheeler, An inkjet printed, roll-coated digital microfluidic device for inexpensive, miniaturized diagnostic assays. *Lab. Chip* **16**(23), 4560–4568 (2016). <https://doi.org/10.1039/C6LC01064D>
28. A.H.C. Ng et al., A digital microfluidic system for serological immunoassays in remote settings. *Sci. Transl. Med.* **10**(438), 6076 (2018). <https://doi.org/10.1126/scitranslmed.aar6076>
29. G. Rosati, M. Ravarotto, M. Sanavia, M. Scaramuzza, A. De Toni, A. Paccagnella, Inkjet sensors produced by consumer printers with smartphone impedance readout. *Sens. Bio-Sens. Res.* **26**, 100308 (2019). <https://doi.org/10.1016/j.sbsr.2019.100308>
30. B. Andò et al., An inkjet printed CO<sub>2</sub> gas sensor. *Procedia Eng.* **120**, 628–631 (2015). <https://doi.org/10.1016/j.proeng.2015.08.755>
31. B. Ando, S. Baglio, C.O. Lombardo, V. Marletta, A. Pistorio, A low-cost accelerometer developed by inkjet printing technology. *IEEE Trans. Instrum. Meas.* **65**(5), 1242–1248 (2016). <https://doi.org/10.1109/TIM.2015.2490998>
32. S. Amendola, A. Palombi, G. Marrocco, Inkjet printing of epidermal RFID antennas by self-sintering conductive ink. *IEEE Trans. Microwave Theory Tech.* **66**(3), 1561–1569 (2018). <https://doi.org/10.1109/TMTT.2017.2767594>
33. K.N. Paracha, S.K.A. Rahim, H.T. Chattha, S.S. Aljaafreh, S. Rehman, Y.C. Lo, Low-cost printed flexible antenna by using

- an office printer for conformal applications. *Int. J. Antennas Propag.* **2018**, 1–7 (2018). <https://doi.org/10.1155/2018/3241581>
34. E. Gieva, G. Nikolov, B. Nikolova, Sheet resistance measurement of inkjet printed layers. 2019 42nd International Spring Seminar on Electronics Technology (ISSE), (Wroclaw, Poland, May 2019), pp. 1–6. <https://doi.org/10.1109/ISSE.2019.8810284>
35. J. Zikulnig, A. Roshanghias, L. Rauter, C. Hirschl, Evaluation of the sheet resistance of inkjet-printed Ag-layers on flexible, uncoated paper substrates using Van-der-Pauw's method. *Sensors* **20**(8), 2398 (2020). <https://doi.org/10.3390/s20082398>
36. T.-H. Joubert, P.H. Bezuidenhout, H. Chen, S. Smith, K.J. Land, Inkjet-printed silver tracks on different paper substrates. *Mater. Today Proc.* **2**(7), 3891–3900 (2015). <https://doi.org/10.1016/j.matpr.2015.08.018>
37. A. Albrecht, A. Rivadeneyra, A. Abdellah, P. Lugli, J.F. Salmerón, Inkjet printing and photonic sintering of silver and copper oxide nanoparticles for ultra-low-cost conductive patterns. *J. Mater. Chem. C* **4**(16), 3546–3554 (2016). <https://doi.org/10.1039/C6TC00628K>
38. C. Beisteiner, B.G. Zagar, A survey of inkjet-printed low-cost sensors. *tm Technisches Messen* **85**(7–8), 504–514 (2018). <https://doi.org/10.1515/teme-2017-0136>
39. Epson Professional Imaging - Color Management Guide. <https://files.support.epson.com/docid/cpd3/cpd39134.pdf>. Accessed 15 Oct 2018
40. Novacentrix®, “Metalon® JS-B25P Conductive Inks for Printed Electronics datasheet.” Mar. 2016. [https://www.novacentrix.com/sites/default/files/pdf/Metalon%20JS-B25P\\_1.pdf](https://www.novacentrix.com/sites/default/files/pdf/Metalon%20JS-B25P_1.pdf)

**Publisher's Note** Springer Nature remains neutral with regard to jurisdictional claims in published maps and institutional affiliations.